Finite Element Investigation of Injury Risks of Immature Pelvis and Femur in Pedestrian Impact

Ming Shen[1], Binhui Jiang[2], Anil Kalra[1], Yajing Shu[3], Runzhou Zhou[1], Xin Jin[1], King H. Yang[1]

1. Bioengineering Center, Wayne State University, Detroit, MI 48201
2. Hunan University, Changsha, China
3. Chongqing University, China

Abstract

Car-to-pedestrian collision is a major cause of injury and death for children. Due to the different anthropometric features of a child compared to an adult, children present more injuries in the pelvic region (including the proximal femur) than adults do. It was hypothesized that the epiphyseal growth plates (GPs) in the hip region may affect the stress distribution and further influence the injury pattern seen in children. To quantitatively address this issue, finite element (FE) simulations of an SUV-to-pedestrian impact was conducted. The human model was built based on a 10-year-old whole-body FE model (CHARM-10) embedded with the GPs at the pelvic region (triradiate cartilages at the bottom of acetabulum) and the proximal femur (femoral head GP and greater trochanter GP). The GP geometries were taken from clinical images and medical study reported in the literature. The material properties were derived from a set of optimization procedures using the published experimental results. The results of the parametric studies revealed that the GPs have significant effects on the mechanical responses and injury outcomes. More specifically, the hip joint contact force was reduced, implying a reduced stiffness of the pelvic girdle; the risks of fractures at the femoral shaft and acetabulum are decreased; the risk of pelvic ramus fracture is elevated. Further simulations explained the detailed effect of each of the three GPs at the hip region.

Introduction

Car-to-pedestrian collision is a major cause of injury and death for children. Due to different anthropometric features of a child compared to an adult, children exhibit a higher rate of injuries in regions around pelvis and proximal femur than adults do [1]. Because of their distinct properties and strength compared to the surrounding bonny structures, the epiphyseal growth plates (GPs) in the hip region may affect the stress distributions and the injury outcomes [2]. These GPs include the triradiate cartilage (TC), femoral head GP (FH GP), greater trochanter GP (GT GP), and ischiopubic ramus GP (*i.e.*, ischiopubic synchondrosis, RM GP), as shown in Fig. 1.

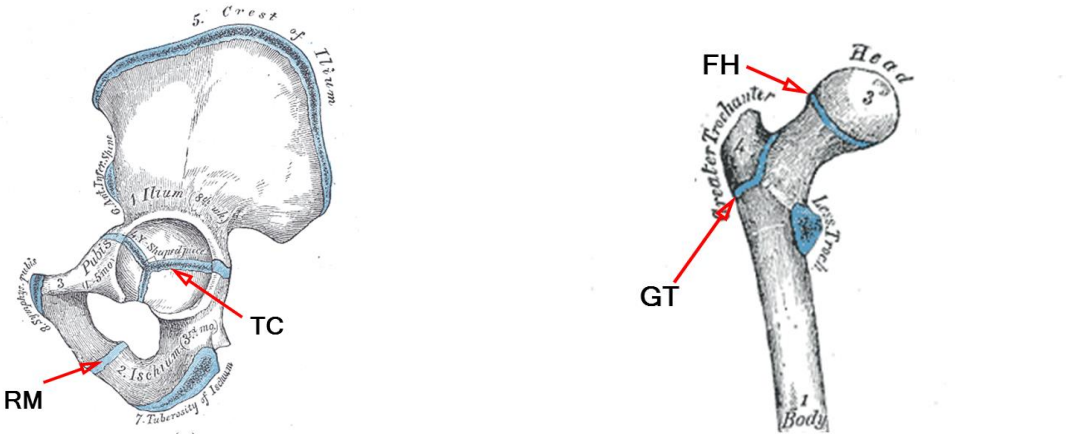

(a) (b)

Fig.1: Anatomy of the GPs in pelvis and femur regions [3]. (a) Lateral view of the left pelvic bone; TC: Triradiate cartilage, Ischiopubic ramus GP (RM GP); (b) Anterior view of the proximal right femur. FH: Femoral head GP; GT: Greater trochanter GP.

The first three GPs are ossified at an age between 14 and 19, while the RM GP ossification age is normally around 4 to 7 years, as summarized in Table 1. Due to this factor, variations in the material properties of some or all of these GPs should be taken into account when studying age dependent pediatric traumatic injuries. By far, no quantitative study has addressed the influences of these GPs in the field of impact biomechanics, in either finite element (FE) modeling or multi-body modeling approach.

TABLE 1: Summary of the GPs at the pelvic region

No.	Name	Closure age
1	triradiate cartilage (TC)	15-18 [4]
2	Femoral head GP (FH GP)	14-19 [5] (for boys)
3	Greater trochanter GP (GT GP)	16-18 [5] (for boys)
4	Ischiopubic ramus GP (RM GP)	4-7 [6]

It has been found that pelvic injury patterns of children and adults are different. For example, Silber and Flynn conducted a 9 years long epidemiologic study based on data available in their trauma center [7]. The fusion of TC was used as the criterion to determine the extent of pelvis maturity. Resulting data revealed that the immature pelvis showed a higher propensity for pelvic ramus fracture and lower propensity for acetabular fracture. More details are illustrated in Fig. 2.

Another study by Von Heyden *et al*. (2012) found a similar trend as seen in [7] that the incidence rate of acetabular fracture for children was much lower than that of adults. Among all pediatric pelvis fracture cases, 9.8% were acetabular fractures in contrast to 22.3% for adults [8].

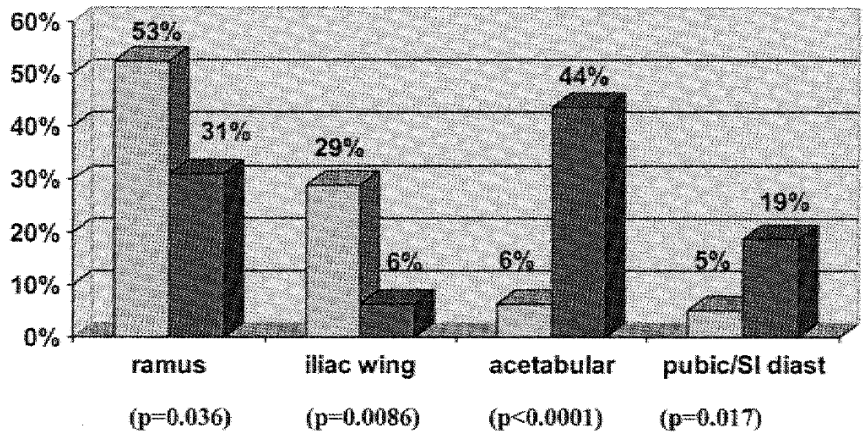

Fig. 2: Percentage distribution of regional fracture pattern between immature (lighter bars) and mature (darker bars) pelvic groups. Figure taken from Silber and Flynn [7].

Relatively speaking, these epidemiologic findings revealed that the immature acetabulum is less likely to be fractured. One possible reason is that the pediatric acetabulum is more compliant due to the presence of TC. In this study, it is hypothesized that the difference in injury pattern between children and adults can be partially explained by the skeletal immaturity in children. To test this hypothesis, the target group selected in this research was the 10-year-old (10YO) age group, because it is one of the most vulnerable groups in pedestrian accidents [9, 10]. At this age, the GPs at TC, FH and GT are not fused, while the RM GP has been fused. Medical images of these three GPs were used to model the geometric features. The material properties were derived from a set of optimization procedures using experimental data reported in the literature. The newly derived geometric features and material properties were then embedded into a whole-body Collaborative Human Advanced Research Models-10 years (CHARM-10) FE model developed at Wayne State University [11]. A typical loading condition mimicking an SUV-to-pedestrian impact was simulated using the updated CHARM-10 model. A series of parametric studies with varying configurations of the GPs were performed to investigate the effects of the GPs on the mechanical responses, including the hip joint contact force and maximum principal strain (MPS) at several critical regions.

Material and Method

10YO baseline model

The baseline CHARM-10 model represents a 10 years old child with a height of 1.40 m and a weight of 35.0 kg. This model has been verified to have reasonable geometric features and mechanical responses at both the component [12-15] and whole-body levels of a 10YO child [11]. Therefore, it is considered a reasonable baseline model for investigations into detailed injuries at the tissue level.

GP geometric study and model update

The computed tomography (CT) scan images at the hip joint of a 10YO child were used to reconstruct the FH GP. As shown in Fig. 3 (a), the shape of GP was clearly recognizable in the CT scans displayed in Mimics (v. 12, Materialise, Leuven, Belgium), although the thickness was not ascertainable. Therefore, the proximal surface was firstly reconstructed using 2D meshes, and then the 2D meshes were dragged in the normal direction to build a 3D plate, as shown in Fig. 3

(b) and (c). The thickness was assumed to be 1.35 mm, which was obtained from the experimental study on human GP samples by William *et al*. [16]. The GP was then embedded to the original model with proper nodal connections to the surrounding structures.

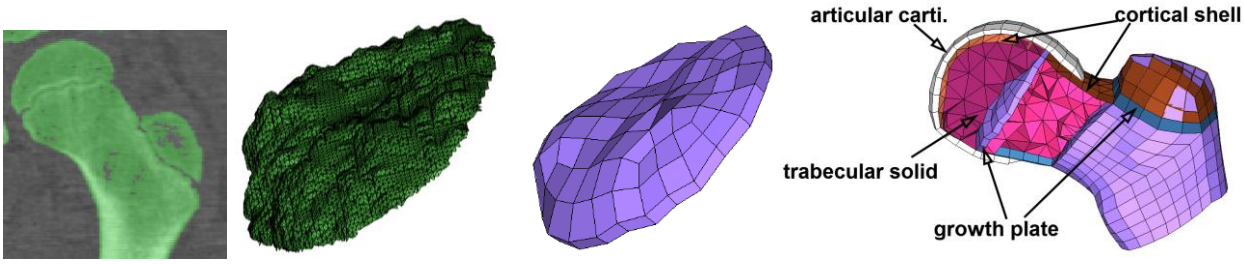

Fig. 3: Reconstruction and modeling of the femoral head (FH) GP. (a) An anterior-posterior view of a CT scan, with the dense regions painted in green color in Mimics; (b) Surface shape reconstruction with original 2D meshes; (c) 3D plate of the FH GP by dragging the pre-meshed 2D surface; (d) GP has been embedded into the baseline FE model of the proximal femur.

The TC and GT GPs were built by replacing layers of solid elements with distinct GP material properties. The updated skeleton in the pelvic region was shown in Fig. 4. All meshing work was done using Hypermesh (v. 12, Altair, Troy, MI).

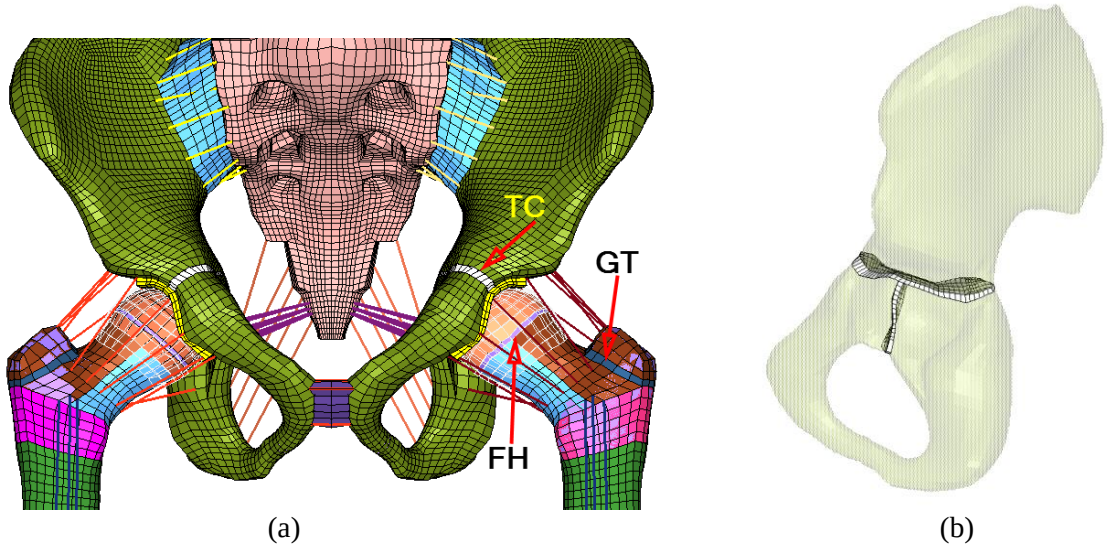

Fig. 4: GPs embedded in the child pedestrian model. (a) An overview of GPs in the pelvic region (frontal view, and the articular cartilages at the femoral head were set as transparent), (b) A lateral view of the left hipbone with TC. TC: Triradiate cartilage; FH: Femoral head GP; GT: Greater trochanter GP.

Material properties and validation

Two experimental studies on testing FH GP samples taken from children around 10YO were found in the literature. Williams *et al*. reported the tensile modulus for bone-GP-bone specimens from an 8YO and a 13YO children [16]. Chung *et al*. conducted femoral capital epiphysis shearing test using whole femur bones from children aged 0 to 15, and reported the shear strength of FH GP for different ages [17]. These data were used to determine the FH GP properties and failure criterion by a set of optimization processes. No such test data are available for other GPs. As such, the GT GP was assumed to have the same properties as the FH GP, and

the TC was assumed to be identical to that of the acetabulum cartilage, since those two are inherently fused together. No failure criterion was assigned to the TC, because the TC failure was rarely reported [8]. The material properties assumed for the main components are listed in Table 2.

TABLE 2: Material properties of major components

Part	Properties	Failure criterion
Articular cartilage	Elastic, E=10 MPa [2] , Thickness=1mm	Max. principal strain: 0.35 (from optimization)
FH GP	Elastic, E=4.26 MPa [16], PR=0.40 [18]	Max. shear strain: 0.53 (from optimization)
GT GP		
TC	Hyperelastic Rubber, as acetabulum cartilage in [15]	None

* E: Young's modulus; PR: Poisson's ratio

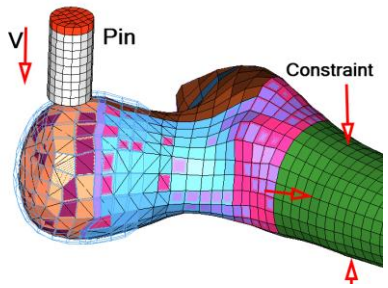

Fig. 5: Validation setup of femoral head GP shearing test, according to Chung *et al*. [17]

TABLE 3: Validation results

	Shear Strength	Pt/Pp*
Chung test	1.20 MPa	1.15
FE model	1.26 MPa	1.19
Error	+4.8%	+3.5%
*Pt/Pp: the ratio of the peak forces for samples with/without surrounding cartilage		

The setup for mimicking the FH GP shearing test is shown in Fig. 5. A steel pin was positioned on the femoral head proximal to the GP and loaded at a speed of 2 mm/min in an anterior-posterior direction, while the femur bone was restricted from motion at a location distal to the femoral neck. The shear strength was calculated by dividing the peak loading force to the effective cross-sectional area and the force ratio for samples with and without the surrounding cartilage was determined. The model-predicted results are shown in Table 3. Overall, the shear strength in the simulation was 4.8% larger and the peak force ratio was 3.5% larger than that of the experimental data. A good match has been observed in this validation.

Simulation setup and experiment design

In the SUV-to-pedestrian impact simulation, the updated child model was standing upright and the SUV struck from the lateral direction at a speed of 5 m/s (Fig. 6). The SUV model was downloaded from the website of NCAC (National Crash Analysis Center) and simplified to represent the front portion of a 2002 Ford Explore. The simulation was performed in LS-DYNA® (v. 971, R 4.2.1, Livermore Software Technology Corporation, Livermore, CA).

Fig. 6: Simulation setup of the SUV-to-pedestrian impact

TABLE 4: Simulation cases

No.	Model configuration
1	Baseline model: No GP
2	Updated model: With all GPs
For detailed effect analysis	
3	Only with TCs
4	Only with FH GPs
5	Only with GT GPs

Table 4 shows the five simulation cases. The original CHARM-10 model (without any GP at the pelvic region) was first used as the baseline model. The updated FE child model was used in the same loading condition, with three GPs embedded (No. 2). To compare the mechanical responses of these two configurations, the contact force at the hip joint on the left side (impact side) was tracked, and the MPS at three critical regions were examined. The three critical regions were the acetabulum bottom, ischiopubic ramus, and the inner side of femoral shaft, which were selected based on the fracture pattern of pelvis and femur observed in the epidemiology studies [7, 8].

To further investigate the detailed effect of each GP in the overall changes observed in the updated model, three additional cases with only one of the three GPs at a time were built (No. 3, 4, and 5). The same responses of the contact force and MPS were tracked.

Results

Baseline model

Contours of the MPS for cortical bones at the pelvis (shell element) and femoral shaft (solid elements) are plotted in Fig. 7. The three most critical sites where fractures may occur are located at: (A) bottom of acetabulum, (B) ischiopubic ramus, and (C) inner side of the femoral shaft. The average MPS of five elements at each site were obtained to evaluate the risk of fracture. It should be noted that all the target elements are not adjacent to the site of GPs, to avoid the local stress concentration.

For the baseline model, the peak joint contact force was 3,059 N. The average MPS's of the cortical shell elements at the acetabulum bottom (A) and ischiopubic ramus (B) were 0.751% and 0.334%, respectively, both below the failure threshold of 2.7% set by the CHARM-10 model. The average MPS of the cortical solid elements at the femoral shaft was 0.934%, also below the preset failure threshold of 2.0%.

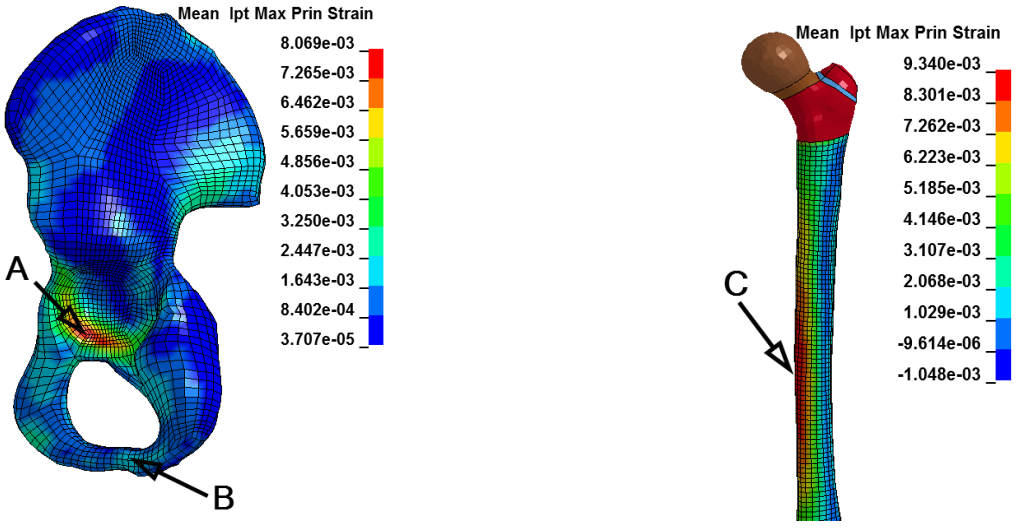

(a) t=12 ms (b) t=14 ms

Fig. 7: The Maximum Principal Srain (MPS) contours of the simulation case No. 1 (without GP presence). The unit of the countour is GPa. Three cirtical regions are: (A) bottom of acetabulum, (B) ischiopubic ramus, and (C) inner side of femoral shaft. Only cortical bone is presented.

Updated model

During the impact simulation using the updated model with all three GPs (Case 2), the FH GP failed at 9.8 ms, due to excessive shear stress, as shown in Fig 8. The reported peak contact force was 2,253 N, which is 26.3% lower than that predicted by the baseline model. The model-predicted MPS values at points A and C were all significantly lower than that observed in the baseline model. The MPS at the acetabulum bottom was 0.346%, which was 53.9% lower than that predicted by the baseline model. The MPS at the inner side of the femoral shaft was 0.697%, which was 25.4% lower than that of the baseline model. The MPS at the ischiopubic ramus (point B) was 0.545%, which was 63.2% higher than the baseline model.

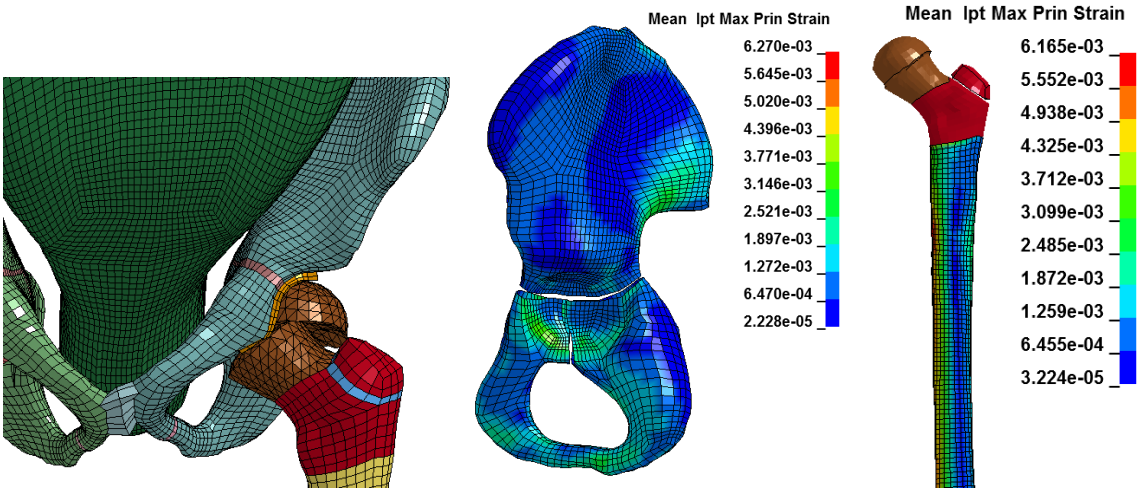

(a) t=12 ms (b) t=10 ms (c) t=10 ms

Fig. 8: Simulation results of the updated 10YO model. (a) The failed FH GP at 10 ms. (b) The MPS distribution of the cortical shell elements of the hip bone. (c) The MPS distribution of the femoral shaft.

The detailed analysis of effect of each GP

The hip joint contact force and the MPS at the three critical locations for cases 3-5 were calculated and compared to the baseline mode (case 1). The percentage differences are shown in Fig. 9.

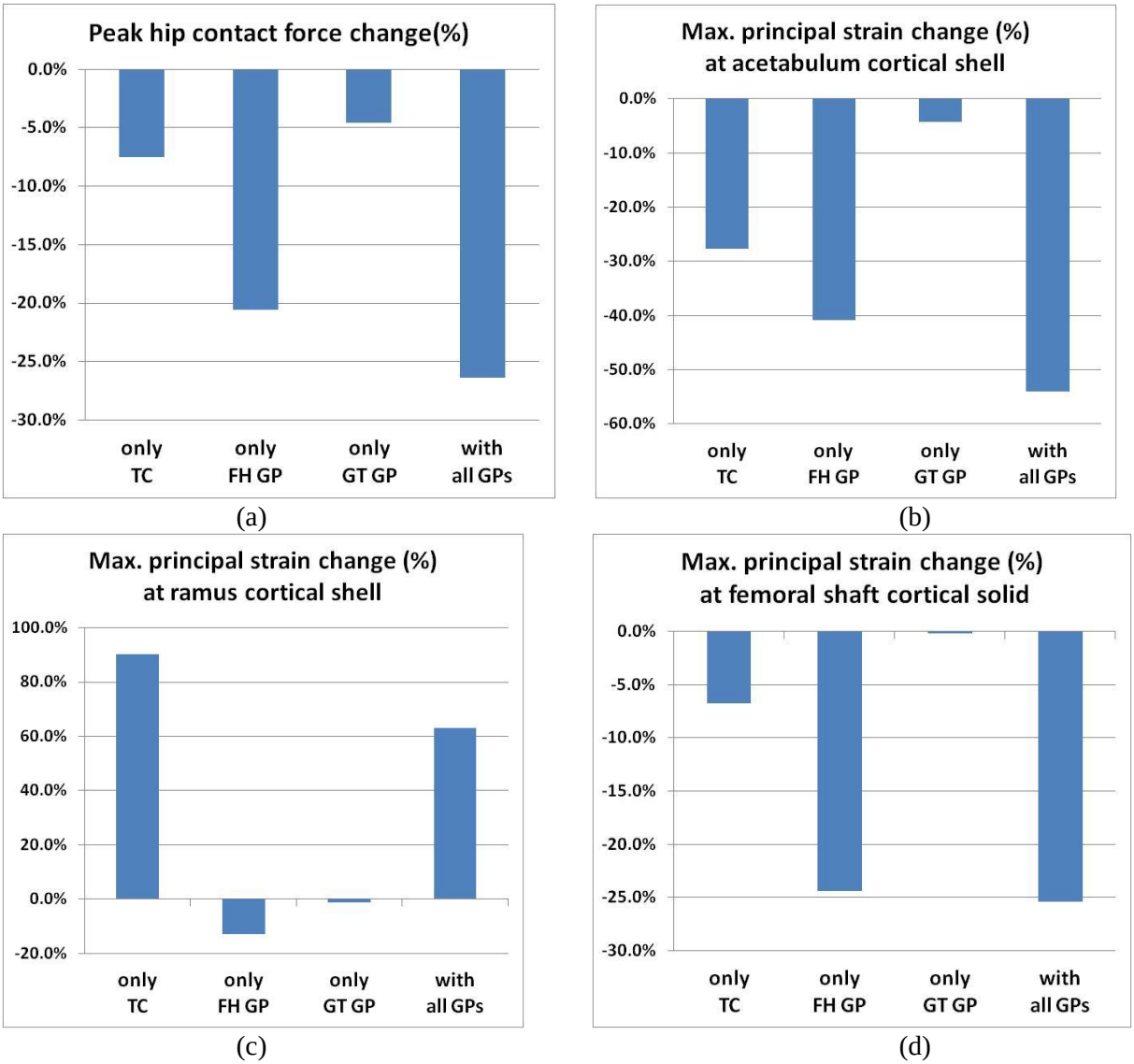

Fig. 9: Simulation results of cases 2-5 compared to case 1. (a) Changes in the peak hip joint contact force; (b) Changes in the MPS at the acetabulum bottom; (c) Changes in the MPS at the ischiopubic ramus; (d) Changes in the MPS at the femoral shaft.

For the peak joint contact force, the insertion of the FH GP alone can reduce it by 20.6%, while all other GPs have minor influences. The case with all GPs shows a 26.3% decrease. The reduced joint contact forces imply a lower stiffness of pelvic girdle in the child body with GPs.

For the MPS at the acetabulum bottom, the TC GP reduced the MPS by 27.7% while the FH GP reduced the MPS by 40.9%. These GPs were the main reasons for the overall reduction in the MPS. For the MPS at the pelvic ramus, the TC drastically increased the MPS by 90.1%, while the other GPs had insignificant negative influences. Overall, the case including all GPs showed a

strong increase in the MPS at the ramus (by 63.2%). For the MPS at the impact side of the femoral shaft, all the GPs showed some reduction effects with the FH GP played a dominant role.

Limitations

There are some limitations in this study. The geometric representation of the GPs is not accurate except the FH GP. Even for the FH GP, the effect due to the roughness of the meshes is unknown. Compared to the setting in the FH GP, which was validated against the experimental data, the lack of data for validating the TC, GT GP, and RM GP could impair the confidence levels of the simulation results. Another limitation is that the validation of the FH GP was against a simple shearing test, which is not identical to the pedestrian impact scenario. Additionally, the material properties of the TC and RM GPs were assumed to be the same as the acetabulum cartilage, because of the unavailability of the experimental data on these GPs. This assumption is only reasonable to a certain extent. The failure of these GPs may change the stress and strain distribution. For example, the MPS of the TC in case 2 can reach 40%, which is close to the failure threshold assumed for the femoral head GP. This high value implies that the failure of the TC may need further investigation, although the TC fracture is not a common injury pattern observed in children.

Conclusion

In this study, the effects of three main GPs at the pelvic region were discussed in a typical SUV-to-pedestrian impact, using an updated 10YO child FE model. The geometry and material properties of the GPs were estimated based on clinical images and experimental data reported in the literature. The simulation results reveal that the presence of GPs may reduce the stiffness of the pelvic girdle and the fracture risks at the acetabulum and the femur, while elevating the risk of the pelvic ramus fracture. All these results match the epidemiology findings well. Our simulation results support the hypothesis that there is a difference in injury pattern between children and adults, and the difference can be partially explained by the skeletal immaturity of a child.

References

1. Serre, T., Lalys, L., *et al.* Child pedestrian anthropometry: evaluation of potential impact points during a crash. *Accident Analysis & Prevention*, 2010, 42 (6): 1943-1948.
2. Cohen, B., Chorney, G. S., *et al.* The microstructural tensile properties and biochemical composition of the bovine distal femoral growth plate. *Journal of Orthopaedic Research*, 1992, 10 (2): 263-275.
3. Gray, H. Gray's Anatomy of Human Body. 1918 (Accessed: 2016 March. 1st); Available from: http://www.bartleby.com/107/57.html.
4. Peterson, H. A. Epiphyseal growth plate fractures. 2007, *Springer*: Heidelberg.
5. Scheuer, L., Black, S., Cunningham, C. Developmental juvenile osteology. 2000, *Academic Press*.
6. Ogden, J. A. Skeletal injury in the child. 3rd ed. 2000, *Springer*: New York.
7. Silber, J. S., Flynn, J. M. Changing patterns of pediatric pelvic fractures with skeletal maturation: implications for classification and management. *Journal of Pediatric Orthopaedics*, 2002, 22 (1): 22-26.
8. Von Heyden, J., Hauschild, O., *et al.* Paediatric acetabular fractures. *Acta Orthopædica Belgica*, 2012, 78: 611-618.
9. Jarrett, K., Saul, R. Pedestrian injury-analysis of the PCDS field collision data. *Proceedings of the 16th International Technical Conference on the Enhanced Safety of Vehicles (ESV)*, 1998, Windsor, Ontario, CA.
10. NHTSA, Traffic Safety Facts 2011 data - Children. *Government Report*, 2013 (DOT HS 811 767).
11. Shen, M., Mao, H., *et al.* Introduction of Two New Pediatric Finite Element Models for Pedestrian and Occupant Protections. *SAE*, 2016 No. 2016-01-1492.
12. Jiang, B., Cao, L., *et al.* Development of a 10-year-old paediatric thorax finite element model validated against cardiopulmonary resuscitation data. *Computer methods in biomechanics and biomedical engineering*, 2014, 17 (11): 1185-1197.
13. Zhou, Z., Jiang, B., *et al.* Numerical simulations of the 10-year-old head response in drop impacts and compression tests. *Computer Methods and Programs in Biomedicine*, 2015, (In press):
14. Dong, L., Li, G., Mao, H., Marek, S., Yang, K. H. Development and validation of a 10-year-old child ligamentous cervical spine finite element model. *Annals of Biomedical Engineering*, 2013, 41 (12): 2538-2552.
15. Shen, M., Zhu, F., *et al.* Finite element modelling of 10-year-old child pelvis and lower extremities with growth plates for pedestrian protection. *International Journal of Vehicle Safety*, 2015, 8 (3): 263-286.
16. Williams, J. L., Do, P. D., Eick, J. D., Schmidt, T. L. Tensile properties of the physis vary with anatomic location, thickness, strain rate and age. *Journal of Orthopaedic Research*, 2001, 19 (6): 1043-1048.
17. Chung, S. M., Batterman, S. C., Brighton, C. T. Shear strength of the human femoral capital epiphyseal plate. *Journal of Bone and Joint Surgery*, 1976, 58 (1): 94-103.
18. Sairyo, K., Goel, V. K., *et al.* Three-dimensional finite element analysis of the pediatric lumbar spine. Part I: pathomechanism of apophyseal bony ring fracture. *European Spine Journal*, 2006, 15 (6): 923-929.